

10-2018

Submarine Deep-Water Lava Flows at the Base of the Western Galápagos Platform

Molly Anderson
Boise State University

V. Dorsey Wanless
Boise State University

Darin M. Schwartz
Boise State University

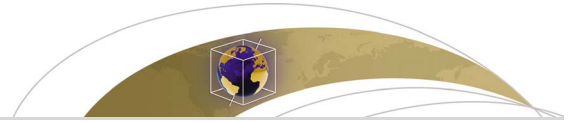
Emma McCully
Boise State University

Daniel J. Fornari
Woods Hole Oceanographic Institution

See next page for additional authors

Authors

Molly Anderson, V. Dorsey Wanless, Darin M. Schwartz, Emma McCully, Daniel J. Fornari, Meghan R. Jones, and S. Adam Soule



Geochemistry, Geophysics, Geosystems

RESEARCH ARTICLE

10.1029/2018GC007632

Key Points:

- Deep-water lava flows at the base of the Galápagos Platform are composed of multiple eruptions, including alkalic and tholeiitic lavas
- Tholeiitic lavas are formed by higher extents of melting and likely pass through the lower portion of the Fernandina magma chamber
- Alkalic magmas are formed by lower extents of melting at the leading edge of the plume and may be analogous to lavas erupted at Loihi Seamount

Supporting Information:

- Supporting Information S1
- Table S1
- Table S2
- Table S3
- Table S4

Correspondence to:

V. D. Wanless,
dwanless@boisestate.edu

Citation:

Anderson, M., Wanless, V. D., Schwartz, D. M., McCully, E., Fornari, D. J., Jones, M. R., & Soule, S. A. (2018). Submarine deep-water lava flows at the base of the western Galápagos platform. *Geochemistry, Geophysics, Geosystems*, 19, 3945–3961. <https://doi.org/10.1029/2018GC007632>


Received 23 APR 2018

Accepted 17 AUG 2018

Accepted article online 4 OCT 2018

Published online 25 OCT 2018

Submarine Deep-Water Lava Flows at the Base of the Western Galápagos Platform

Molly Anderson¹, V. Dorsey Wanless¹ , Darin M. Schwartz¹, Emma McCully¹, Daniel J. Fornari², Meghan R. Jones² , and S. Adam Soule²

¹Department of Geosciences, Boise State University, Boise, ID, USA, ²Geology and Geophysics Department, Woods Hole Oceanographic Institution, Woods Hole, MA, USA

Abstract To investigate the initial phases of magmatism at the leading edge of the upwelling mantle plume, we mapped, photographed, and collected samples from two long, deep-water lava flows located at the western base of the Galápagos Platform using the remotely operated vehicle *Hercules*. Lavas were recovered from four areas on the seafloor west of Fernandina volcano, including the western flow fronts of two deep-water flows, heavily sedimented terrain between the two flows, and the eastern, shallower end of one flow. The sediment cover and morphologies are distinct between the western flow fronts and the eastern region based on seafloor imagery, suggesting that the long lava flows are not a single eruptive unit. Major and trace element concentrations reveal both tholeiitic and alkalic compositions and support the interpretation that multiple eruptive units comprise the deep-water flows. Alkalic lavas have higher [La/Sm]_N ratios (2.05–2.12) and total alkali contents (5.18–5.40) compared to tholeiitic lavas, which have [La/Sm]_N ratios ranging from 1.64 to 1.68 and total alkali contents ranging from 3.07 to 4.08 wt%. Radiogenic isotope ratios are relatively homogeneous, suggesting a similar mantle source. We use petrologic models to assess three alternative mechanisms for the formation of the alkalic magmas: (1) high-pressure crystallization of clinopyroxene, (2) mixing of high silica and mafic magmas, and (3) variable extents of melting of the same mantle source. Our modeling indicates that the alkalic samples form from lower extents of melting compared to the tholeiitic lavas and suggests that the deep-water alkalic lavas are analogous to the initial, preshield building phase observed south of Hawaii and at the base of Loihi Seamount.

1. Introduction

The current Galápagos Islands, located on the Nazca plate ~1,000 km west of Ecuador, have been constructed over the past ~4 Ma by volcanic eruptions associated with melting of an upwelling mantle plume (e.g., McBirney & Williams, 1969; White et al., 1993). The Galápagos are atypical for an ocean island system in that most of the subaerial volcanoes are built on top of a large (~3,500 km²), shallow volcanic platform that stands ~3,000 m above the surrounding seafloor (Figure 1; Geist et al., 2008). The platform consists of stacked lava terraces that can each be hundreds of meters thick and are geochemically similar to lavas erupted at adjacent subaerial volcanoes (Geist et al., 2006, 2008). The construction of this platform likely precedes island formation for all modern islands in the archipelago (Geist et al., 2006).

Platform and terrace construction processes in the Galápagos have been deduced from interpretations of side scan sonar and bathymetric data from the seafloor west of Fernandina Island (Geist et al., 2006, 2008). These studies identified several highly reflective (i.e., unsedimented and presumed young), long (up to 30 km in length), deep-water (>3,000-m depth) lava flows (DWFs) on the seafloor at the western edge of the platform (Figures 1 and 2). Combining observations of DWFs and terrace flows led Geist et al. (2008) to hypothesize that the platform is constructed from repeated eruptions of long lava flows at the western, leading edge of the Galápagos hotspot, which stack and coalesce to form the thick volcanic terraces. Thus, the DWFs at the leading edge of the Galápagos platform are thought to represent the initial phases of platform construction and may be analogous to DWFs at the base of Loihi Seamount's south rift zone, at the leading edge of the Hawaiian hotspot (e.g., Lipman & Calvert, 2013; Moore et al., 1982).

To assess the magmatic and eruptive processes leading to the formation of the long lava flows, we utilize visual observations and samples from two DWFs (#1 and #2) west of Fernandina Island (Figure 2) using the *E/V Nautilus* and the Ocean Exploration Trust's remotely operated vehicle (ROV) *Hercules*. We first present information pertaining to the morphology and sedimentation on and around the DWFs, based on analysis

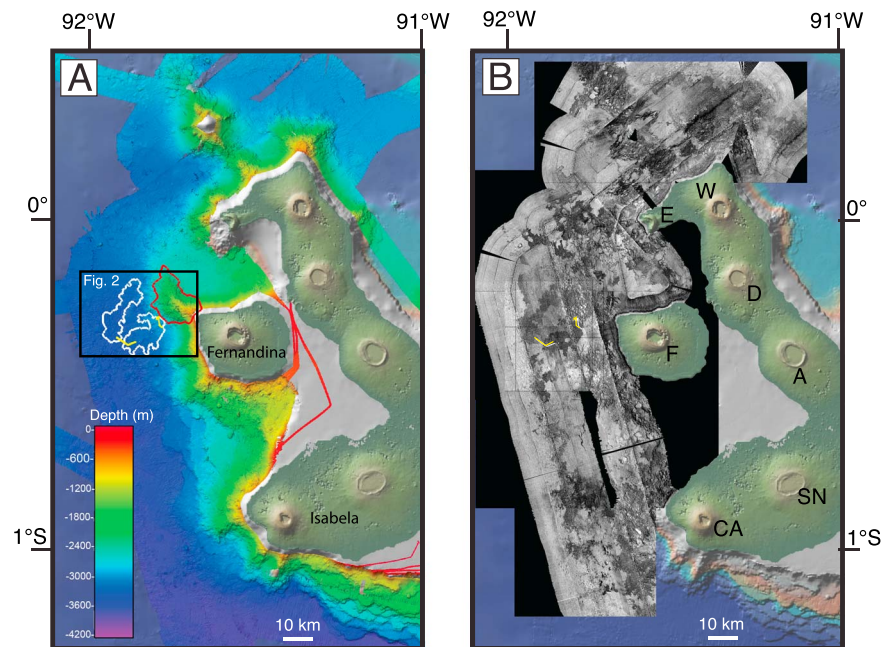


Figure 1. (a) Bathymetric and (b) side scan sonar maps of the Galápagos deep-water lava flow study site; data from Geist et al. (2006). Subaerial Galápagos Islands are shown in green and labeled in black and the shallow platform top is shown in gray. White polygon in (a) denotes the two deep-water lava flows investigated in this study, the red polygon in (a) outlines Fernandina volcano's northwest submarine rift zone, yellow lines show the dive track of remotely operated vehicle *Hercules*, and black box indicates location of Figure 2. Volcanoes on each island in (b) are labeled in black (F=Fernandina; E = Ecuador; W = Wolf; D = Darwin; A = Alcedo; SN = Sierra Negra; CA = Cerro Azul), and yellow lines show the dive tracks of remotely operated vehicle *Hercules*.

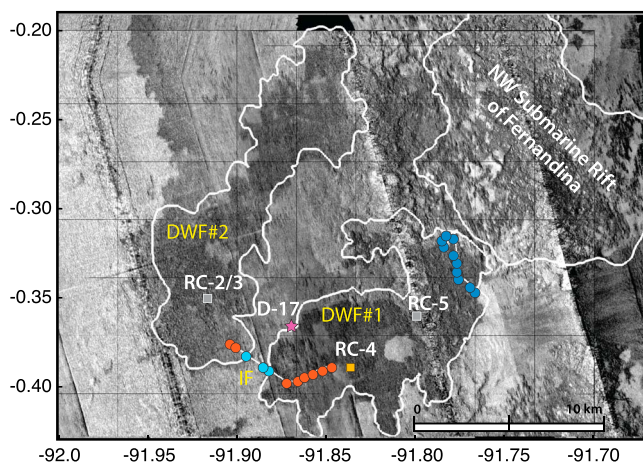


Figure 2. Side scan sonar map of the seafloor west of Fernandina volcano (Geist et al., 2006). The deep-water lava flows (DWFs; dark areas of high reflectivity) are located ~10 km west of Fernandina. The two deep-water flows investigated in this study (DWF#1 and DWF#2) are outlined in white along with another highly reflective uninvestigated portion of the northwest submarine rift zone of Fernandina. Sample locations are shown as circles, with red indicating alkalic samples and blue indicating tholeiitic samples (interflow [IF] tholeiites in light blue). Sample locations from the R/V *Melville* AHA-Nemo2 and R/V *Revelle* DRIFT4 cruise (Geist et al., 2006) are shown as gray (tholeiitic) and orange (alkalic) squares (rock cores [RC]) and a pink star for the single dredge sample of mixed composition (D).

of digital still photography and video footage, from which we provide estimates of relative ages between and along each flow. We use major and trace element contents, as well as radiogenic isotope ratios, to show that the DWFs are compositionally heterogeneous, and include both alkalic and tholeiitic lavas, suggesting that the flows are composed of multiple eruptive units. Finally, we evaluate the petrogenesis of both lava types and present a model for the origin of alkalic and tholeiitic magmas that formed the deep-water flows in the context of ocean island evolution in the Galápagos.

2. Previous Studies of the Seafloor West of Fernandina

In 2001, two research cruises (R/V *Melville* AHA-Nemo2 and R/V *Revelle* DRIFT4) investigated the submarine flanks, terraces, and seafloor south and west of Fernandina, Isabela, and Floreana Islands to better understand the earliest stages of Galápagos volcanism and platform formation (Geist et al., 2006, 2008; Figure 1). Using MR1 surface towed side scan sonar backscatter imagery gridded at 8-m resolution (Rognstad, 1992), Geist et al. (2006, 2008) identified regions of high reflectivity (relatively unsedimented hard-rock surfaces) on the seafloor and interpreted these as long lava flows in the deep water (~3,300–3,500 m) up to 30 km in length with areal extents of ~5–30 km² and thickness estimates of <5 m (Geist et al., 2006). These DWFs traversed relatively flat seafloor at the base of the platform and, due to their low relief, are not resolved by existing multibeam bathymetry (10- to 20-m vertical resolution). The DWFs, with higher reflectivity than the surrounding seafloor, represent the youngest volcanic deposits

in the region, but the patterns of reflectivity throughout the area suggest diverse acoustic facies that could imply a range of ages for the flows (Figure 1b). Some of these large DWFs appear to originate from Fernandina's northwest submarine rift zone (Geist et al., 2006) or volcanic cones in the middle to lower south flank of the northwest rift, while others have no obvious connection to the rift zone (Glass et al., 2007).

The seafloor, terraces, and rift zones west of Fernandina and south and west of Isabela were sampled during the AHA-Nemo2 and DRIFT4 cruises using short-traverse dredging and wax coring. Major element geochemistry of the dredge samples collected from the entire region was presented in Geist et al. (2006). They divided the submarine lavas into three categories based on composition: (1) normal, (2) evolved, and (3) high-K lavas. The majority of the dredged lavas are "normal" tholeiitic basalts and are characterized by relatively high MgO (5.0–7.6 wt%), low K₂O (0.38–0.77 wt%), and abundant plagioclase and olivine antecrysts. These submarine tholeiitic lavas are compositionally similar but more crystal rich compared to subaerially erupted lavas on Fernandina (Geist et al., 2006). The "evolved" submarine lavas, collected along the SW rift zone of Fernandina and the western ends of the DWFs, are characterized by lower MgO (3.19–5.00 wt%) and higher K₂O (>1.5 wt%) compared to the normal series and contain clinopyroxene (CPX), olivine, and plagioclase phenocrysts. The "high-K" lavas are characterized by MgO and SiO₂ contents similar to the normal series but have higher incompatible element values (e.g., K₂O > 1 wt%) for a given MgO content. These lavas were interpreted to be a product of mixing between the evolved and normal lavas (Geist et al., 2006). Both the evolved and high-K series are alkalic, based on total alkali contents versus silica (Figure 3a).

The above descriptions by Geist et al. (2006) are based on sampling that were primarily focused on the submarine rift zones and terraces, with very limited geochemical data from the DWFs. However, a single dredge (D-17; Figure 2) that crossed DWF#1 (Figure 2) and three rock cores (RC-02, RC-04, and RC-05) all collected small chips of glass from DWF#1 and DWF#2 (Figure 2). Major element contents from these dredges and rock cores are reported in Geist et al. (2006), but no trace element contents were measured, due to inadequate sample volumes. Dredge D-17 on the edge of DWF#1 only recovered a few small glass chips in the burlap of the dredge but included both tholeiitic (MgO = 5.85–6.69 wt%; K₂O = 0.45–0.59; Figure 3) and alkalic (MgO = 4.48 wt%; K₂O = 1.69; Figure 3) compositions (Geist et al., 2006). RC-02 on DWF#2 (MgO = 7.42 wt%; K₂O = 0.48) and RC-05 on DWF#1 (MgO = 6.36 wt%; K₂O = 0.57) are tholeiitic, while RC-04 on the western edge of DWF#1 (MgO = 4.51 wt%; K₂O = 1.63) is alkalic (Figure 3). Unfortunately, due to the low relief across the flows, dredges from the previous field programs were not able to collect sufficient samples to corroborate the extents of mapped flows and determine the extent of the alkalic lavas relative to the more normal dredged tholeiites.

3. ROV Dives and Observations

Two ROV dives (*Hercules* 1441 and 1442) were conducted in July 2015 from the E/V *Nautilus* (Carey et al., 2016) to explore the seafloor west of Fernandina. Each dive lasted approximately 15 hr and covered ~8–12 km of seafloor (Figure 2). Navigation of the ROV was accomplished using ultrashort baseline acoustic navigation integrated with ship-based satellite navigation resulting in geodetic precision of ~10 m.

Nearly 10,000 images of the seafloor were acquired during the ROV dives using a Multidisciplinary Instrumentation in Support of Oceanography (MISO) GoPro™ 12-megapixel digital deep-sea camera provided by the Woods Hole Oceanographic Institution (WHOI) MISO Facility (www.whoi.edu/miso). Images were analyzed using a MATLAB™-based graphical user interface to characterize the type of lava morphology and sediment abundance. In addition, new multibeam bathymetric data acquired by the E/V *Nautilus* were gridded at ~50-m pixel resolution and used to correlate features observed in the 8-m-gridded MR1 side scan sonar data with seafloor slope and features observed during the dives (Figure 4).

The dives characterized and sampled lavas from four areas on the seafloor west of Fernandina: (1) the deep, terminal portions of highly reflective DWF#2; (2) a narrow, less reflective area in between the two DWFs; (3) deep, terminal portions of highly reflective DWF#1; and (4) the upper, shallower section of DWF#1 (Figures 1 and 2). Although our results suggest that DWF#1, and possibly DWF#2, comprise multiple lava flows, we still refer to them as flows #1 and #2 for consistency with previous studies (e.g., Geist et al., 2006). Twenty-five basalts were collected from these regions during the 2015 cruise; two basalts were collected from the

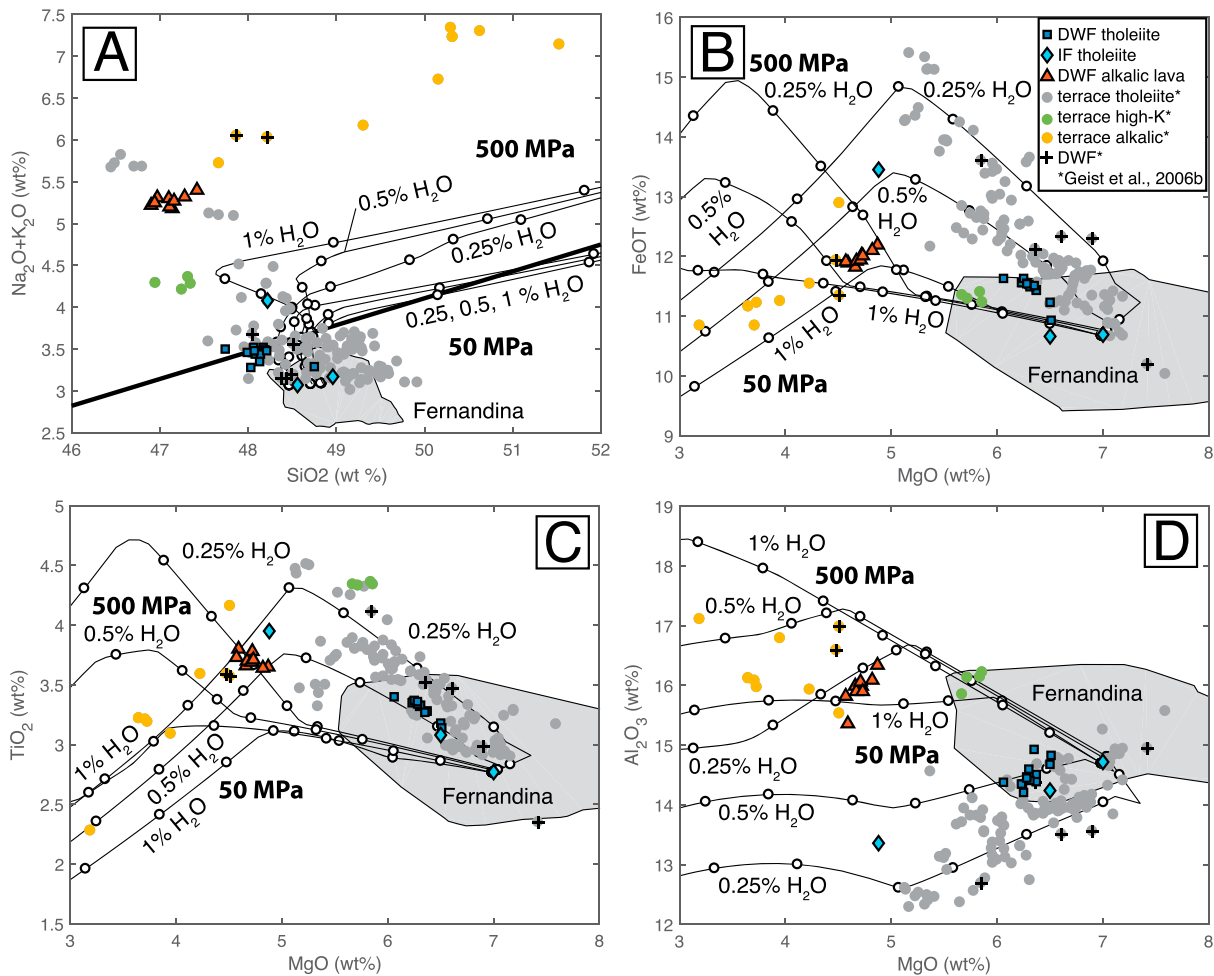


Figure 3. (a) TAS diagram and (b–d) selected harker diagrams for DWF glasses (diamonds, squares, and triangles), compared with Geist et al. (2006) dredged glasses from the DRIFT4 cruise (green, gray, orange circles). Bold line in the TAS diagram represents the boundary between alkalic and tholeiitic compositions (Macdonald & Katsura, 1964). Geist et al. (2006) samples from the two DWFs are indicated by “+.” Modeled fractional crystallization lines on harker diagrams (black lines with white circles) generated from MELTs at 50 and 500 MPa with variable water contents (Ghiorso & Sack, 1995; Smith & Asimow, 2005). White circles indicate 5% crystallization increments on each trend. See text for modeling details. TAS = total alkalis versus silica; DWF = deep-water lava flow; IF = interflow.

terminus of DWF#2, three basalts were sampled from the heavily sedimented seafloor between flows, seven basalts were collected from the western terminus of DWF#1, and 13 basalts were collected from the northeastern, shallow portion of DWF#1 (Figure 2).

Analyses of the digital still imagery suggest a difference in morphology, sediment cover, and thus age between the deeper flow fronts of both DWFs, the area between the flows (interflow [IF]), and the shallower, eastern portion of DWF#1 (Figure 4). The IF region was nearly 100% sediment with a few sparse pillow outcrops (supporting information Figure S1b), suggesting that these lavas are older than the adjacent DWFs. The terminal flow fronts of DWF#1 and DWF#2 are composed of heavily sedimented pillow lavas (Figures S1a, S1c, and S1d), while the upper section of DWF#1 is composed of pillow, lobate, and sheet lava flows, with variable but thinner sediment cover (Figures S1e and S1f). Thus, the upper section of DWF#1 is inferred to be younger than the deeper flow front due to less sediment cover, despite similar slopes (Figure 4). Although pillow lavas are the dominant lava morphology in all regions (Figure 4), the upper section of DWF#1 is also composed of lobate and sheet flows (Figure S1), suggesting higher eruption or flow rates (Gregg & Fink, 1995). Further, we observed a prominent collapse crater ~60 m in diameter and ~30 m deep with fresh, glassy pillow lava at the rim and exposed cross-sections of the flows contained in this shallower portion of DWF#1 (Figure S2).

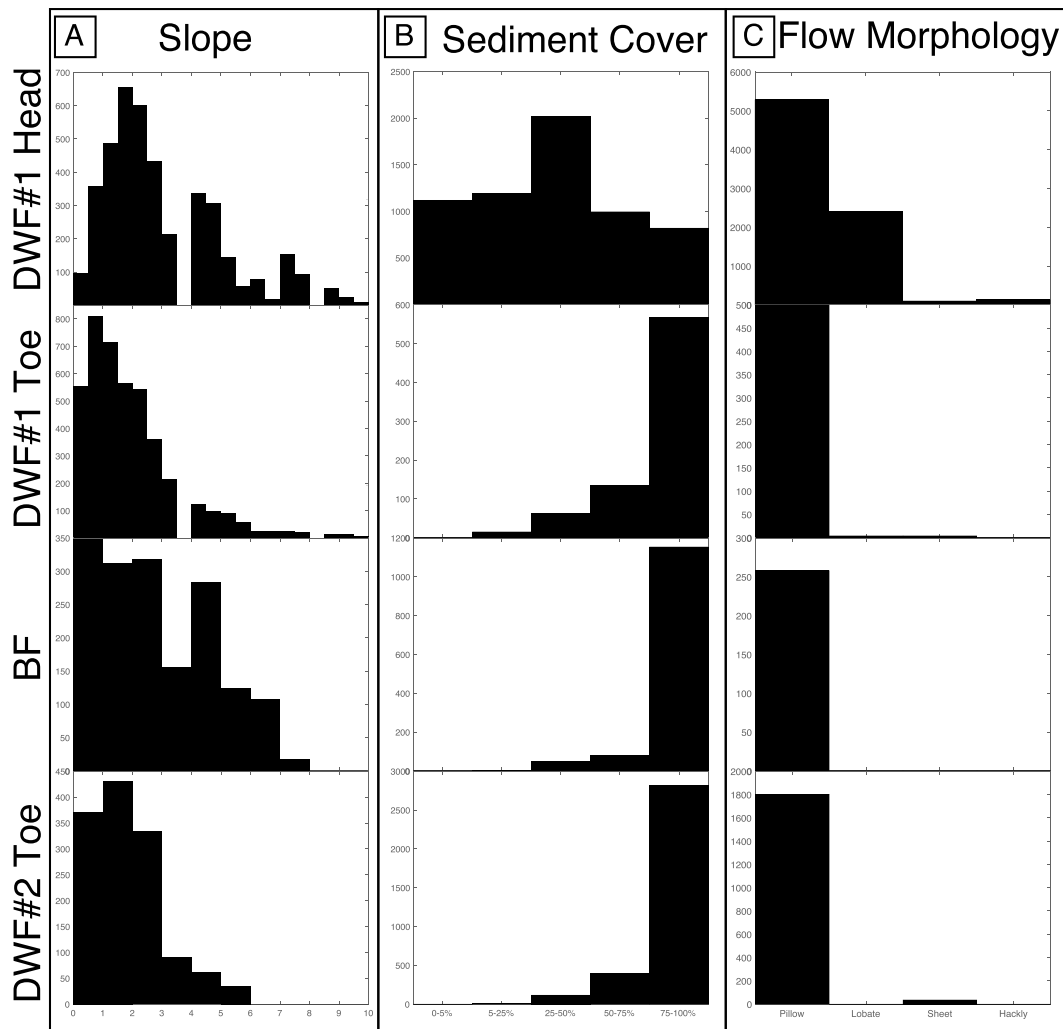


Figure 4. Morphology statistics from map and digital image analysis. (a) Histogram of seafloor slope along each dive traverse. (b) Histogram of sediment cover along each dive traverse. (c) Histogram of lava flow morphology along each dive traverse. The head of DWF#1 has a lower sediment cover and a higher number of lobate, sheet, and hackley flow observations than the other regions despite being composed of similar bathymetric slopes.

4. Geochemical Methods

Basaltic glass was chipped from the outer edge of each sample, and individual chips were handpicked for geochemical analyses using a binocular microscope, avoiding phenocrysts and alteration. The chips were cleaned in an ultrasonating bath of deionized water three times for 30 min to remove alteration and salt precipitates. Major element concentrations (Table S1) of glasses were determined using the Cameca SX Five electron microprobe at Boise State University. The accelerating voltage was 15 kV, beam current was 10 nA, and beam diameter was 10 μm . Count times varied for different elements: S was measured for 60 s; Al, K, and Mg were measured for 50 s; Si and Ca were measured for 40 s; Ti, Fe, and P were counted for 30 s; and Na and Mn were counted for 20 s. To reduce volatile loss, Na and then K were analyzed first. Five spots were measured on each glass and averaged. Basalt standard VG-2 and internal standard 2392-9 (Perfit et al., 2012) were run approximately every seven samples to account for instrument drift. Standard values can be found in the supporting information (Table S1).

All 25 samples were measured for trace element contents using solution inductively coupled plasma mass spectrometer (ICP-MS) at Boise State University (Table S2). Samples were prepared for analysis following methods modified from Kelley et al. (2003) and Lytle et al. (2012). Description of modifications to the dissolution processes can be found in (Schwartz et al., 2018). Trace element concentrations were determined using a

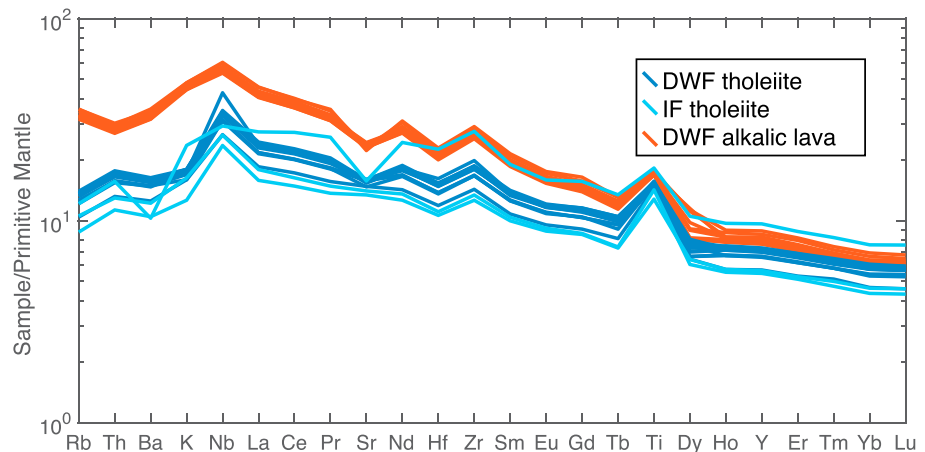


Figure 5. Primitive mantle-normalized trace element diagram for DWF glasses (normalized using McDonough & Sun, 1995). Note the difference in REE patterns between the tholeiitic and alkalic samples, where alkalic lavas are more enriched in LREEs than the tholeiitic lavas. DWF = deep-water lava flow; REE = rare earth element; LREE = light rare earth element; IF = interflow.

ThermoElectron X-Series II Quadrupole ICP-MS at Boise State University. Each solution was measured three times and averaged. The internal standard correction ^{115}In was applied to each analysis. Instrument drift was accounted for by assessing the standards before and after the sample runs. The blank was 8 N HNO_3 , and the standards used included BHVO-2, BIR-1, DNC-1, JB-3, and W-2. Standard values can be found in the supporting information. Radiogenic isotopic ratios were collected on 12 samples at the University of Florida (Table S4). Samples were prepared following methods of Goss et al. (2010). Pb, Sr, and Nd isotopes were then measured at the University of Florida using a Nu-Plasma multicollector ICP-MS.

Volatile concentrations were measured on all 25 samples (Table S3) at the Northeast National Ion Microprobe Facility at the WHOI using a Cameca 1280 secondary ion mass spectrometer, following methods developed by Hauri et al. (2002). Glass from each sample was chipped, cleaned, and hand-polished using a range of grits on silica carbide sandpaper. The glass was then mounted in indium and polished using 6-, 3-, and 1- μm diamond suspension followed by 1- μm alumina suspension. The mounts were dried, gold coated, and stored in vacuum prior to analysis. The measurements were acquired using a 1-nA Cs^+ beam over a 30- μm raster size on vesicle and crystal-free areas. The accuracy and precision for these conditions at WHOI is 10% (2σ). Counting times of 10 s were used over five acquisition blocks after 2 min of presputtering. Measurements with $>10\%$ standard deviation over the five acquisition blocks or with anomalous ^{12}C intensity during analysis were interpreted to reflect surface contamination and discarded. Drift was monitored by repeat measurements on basaltic glass 519-4-1 (Hauri et al., 2002). Standard values can be found in the supporting information (Table S3).

5. Results

5.1. Major and Trace Element Contents

Based on total alkali contents versus silica (Figure 3a), both tholeiitic and alkalic lavas are observed, which have distinct major (Table S4 and Figures 3b–3d) and trace element contents (Table S2 and Figure 5). Tholeiitic basalts were sampled from the shallow eastern edge of DWF#1 and between the two DWFs (IF lavas). The DWF tholeiites are depleted in total alkali contents ($\text{Na}_2\text{O} + \text{K}_2\text{O} = 3.28\text{--}3.52$ wt%) and have low $[\text{La}/\text{Sm}]_N$ (1.64–1.68), K/Ti (0.21–0.23), and $[\text{Sm}/\text{Yb}]_N$ (2.26–2.32; Figure 5). These lavas are characterized by relatively high MgO (6.06–6.51 wt%), SiO_2 (47.74–48.75 wt%), and CaO (10.68–11.08 wt%) contents and low K_2O (0.48–0.54 wt%) and Al_2O_3 (14.21–14.93 wt%) contents compared to other DWF lavas (Figures 3 and S3). The IF lavas are also tholeiitic in composition but are more variable in total alkali content (3.07–4.08 wt%) and other major elements ($\text{MgO} = 4.88\text{--}7.00$ wt%, $\text{CaO} = 9.44\text{--}11.66$ wt%, and $\text{K}_2\text{O} = 0.38\text{--}0.71$ wt%), compared to the DWF tholeiites (Figure 3). These lavas also have more variable

[La/Sm]_N (1.40–1.67), K/Ti (0.19–0.25), and [Sm/Yb]_N (2.11–2.45; Figure 5). The most extreme trace element variability in the IF lavas arises from NA064-075 with a distinct trace element pattern (Figure 5).

The western (deeper) basalts from both DWFs have higher total alkalis (Na₂O + K₂O = 5.18–5.40 wt%) compared to the tholeiitic samples from the previous groups and are described together due to similarity in composition. In addition to higher alkali contents, these lavas have higher minor (K/Ti = 0.50–0.54) and trace element ratios ([La/Sm]_N = 2.06–2.12, [Sm/Yb]_N = 3.04–3.11). Alkalic lavas, collected from the western end of both DWFs, have relatively low MgO (4.57–4.87 wt%), SiO₂ (46.90–47.42 wt%), and CaO (8.59–8.84 wt%) and high K₂O (1.34–1.45 wt%) and Al₂O₃ (15.36–16.34 wt%) contents compared to the tholeiitic lavas (Figure 3).

5.2. Volatile Concentrations

The alkalic lavas display similar dissolved CO₂ concentrations (107–136 ppm) and higher dissolved H₂O (1.15–1.65 wt%), F (799–1,323 ppm), Cl (799–1,323 ppm), and S (1,721–1,911 ppm) concentrations than the tholeiitic lavas from DWF#1 (111–157 ppm CO₂; 0.083–1.09 wt% H₂O; 515–592 ppm F, 239–280 ppm Cl, 1,271–1,729 ppm S; Figure S4). Excluding CO₂, the IF tholeiitic lavas display more variable dissolved volatile concentrations than tholeiites from DWF#1 (158–171 ppm CO₂, 0.60–1.08 wt% H₂O, 393–821 ppm F, 234–272 ppm Cl, and 1,386–1,888 ppm S). Similar to the trace element geochemistry, the variability in the volatile concentrations of the IF lavas arises from sample NA064-075.

5.3. Radiogenic Isotope Ratios

All of the lavas (including both alkalic and tholeiitic basalts) are isotopically similar (Figure 6), with the exception of one anomalous sample, NA064-075, compared to the archipelago-wide variations that have been observed (e.g., Saal et al., 2007). Excluding sample NA064-075, ⁸⁷Sr/⁸⁶Sr ratios range from 0.70319 to 0.70324, and ¹⁴³Nd/¹⁴⁴Nd ratios vary from 0.512932 to 0.512971. ²⁰⁶Pb/²⁰⁴Pb ratios range from 19.047 to 19.124, ²⁰⁷Pb/²⁰⁴Pb ratios range from 15.545 to 15.559, and ²⁰⁸Pb/²⁰⁴Pb ratios range from 38.624 to 38.746. Note that the alkalic and tholeiitic samples form tightly clustered and distinct groups in Pb isotope space and have more depleted thorogenic (²⁰⁸Pb/²⁰⁴Pb) compared to uranium Pb isotope ratios (²⁰⁶Pb/²⁰⁴Pb; Figure 6a). Relative to the other samples from the study, NA064-075 (IF lava) is depleted in all radiogenic isotope ratios (⁸⁷Sr/⁸⁶Sr = 0.702755, ¹⁴³Nd/¹⁴⁴Nd = 0.513042, ²⁰⁶Pb/²⁰⁴Pb = 18.808, ²⁰⁷Pb/²⁰⁴Pb = 15.526, and ²⁰⁸Pb/²⁰⁴Pb = 38.285) and has the most elevated εNd value (7.88 compared to 5.74–6.50).

5.4. Petrography

The alkalic and tholeiitic DWF and IF lava series are petrographically distinct and contain abundant phenocrysts. Based on 500-point counts, tholeiites from the DWF include ~5% olivine (~1 mm) and ~15% plagioclase phenocrysts (1–4 mm), in addition to olivine and plagioclase microphenocrysts (<0.5 mm). IF tholeiites have higher olivine (~10–20%) and lower plagioclase (~5%) phenocryst abundances compared to the DWF tholeiites and also contain olivine and plagioclase microphenocrysts. The alkalic DWF lavas are sparsely plagioclase phyric, containing ~3% plagioclase (1–4 mm) and abundant plagioclase microphenocrysts. Olivine phenocrysts are not observed in the alkalic lavas. This variability in phenocryst contents relative to composition is consistent with results from Geist et al. (2006).

6. Discussion

6.1. Comparison to Previous Studies

The normal series tholeiitic lavas previously dredged from the terraces and rift zones west of Fernandina volcano (Geist et al., 2006) and the tholeiitic DWF lavas in this study are compositionally similar and likely originate from the same magmatic system. Total alkali (Na₂O + K₂O) contents of the DWF tholeiites overlap the normal series (Figure 3a) and fall within the field of normal series lavas in all major element diagrams (CaO, Al₂O₃, FeO_{total}, SiO₂, K₂O, Na₂O, P₂O₅; Figures 3 and S3). Trace element contents of the tholeiitic DWFs are also similar to the dredged normal series basalts (Geist et al., 2006) and radiogenic isotopes fall within the range observed at Fernandina (Figure 6; e.g., Saal et al., 2007). The DWF alkalic lavas are similar in composition to previously dredged (evolved) lavas (Geist et al., 2006); however, the alkalic DWFs have lower total alkalis and silica contents (Figure 3a). The DWF tholeiites exhibit dissolved volatile

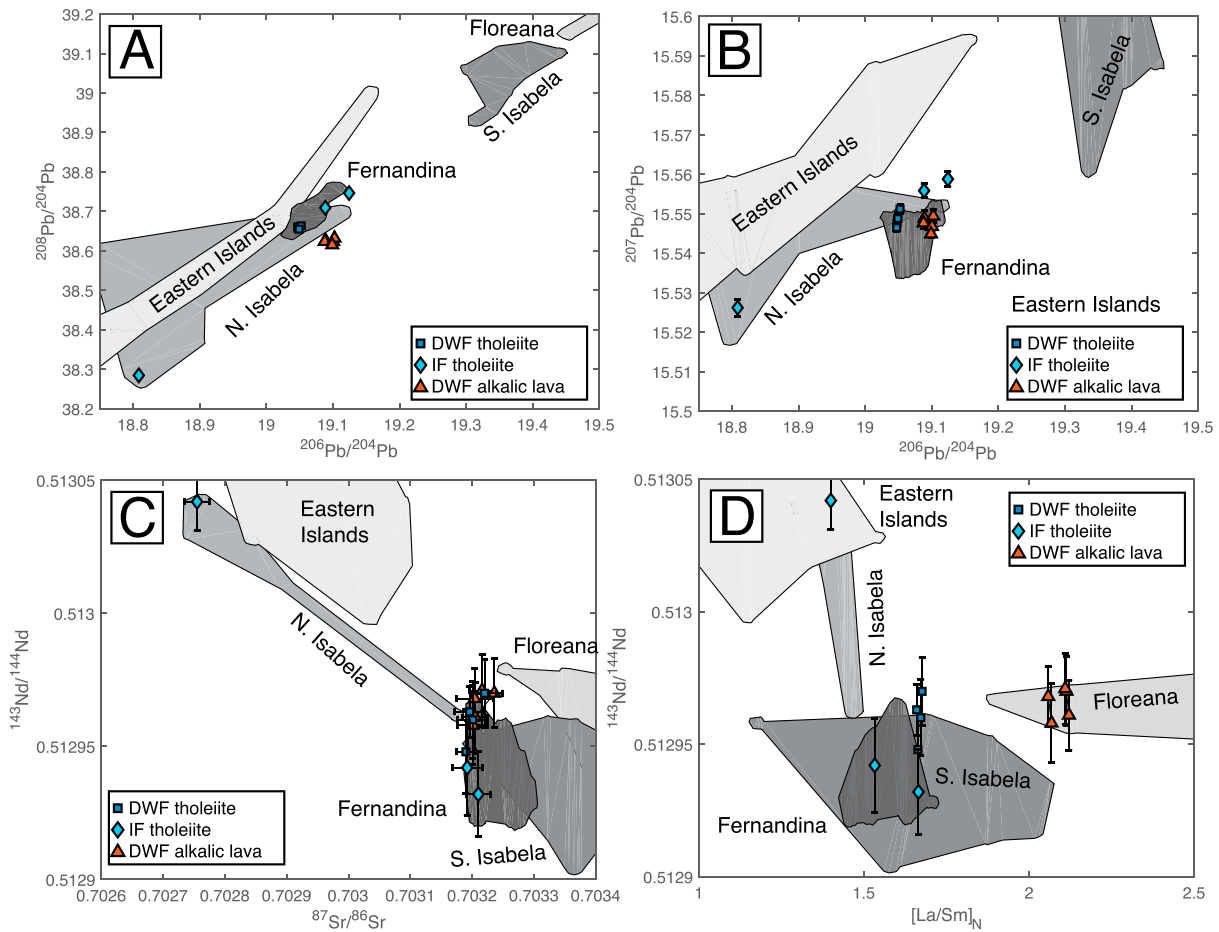


Figure 6. (a–c) Radiogenic isotope (Pb, Sr, and Nd) ratios and (d) $[La/Sm]_N$ -against-Nd ratio for the DWFs. Regional Galápagos basalt fields are provided for comparison as grayscale polygons (Eastern Islands, Isabela, and Fernandina data from Saal et al., 2007; Floreana data from Harpp et al., 2014). Error bars are shown as 2σ . DWF = deep-water lava flow; IF = interflow.

concentrations similar to Fernandina group lavas from Peterson et al. (2017), while the alkalic lavas display higher dissolved H_2O , F, Cl, and S concentrations than previously studied submarine basalts from the Galapagos (Peterson et al., 2017; Figure S4). Similar to previously studied submarine Galapagos lavas, the DWF samples range from slightly sulfide undersaturated to sulfide saturated (Peterson et al., 2017; Fortin et al., 2015) and display dissolved H_2O and CO_2 concentrations consistent with equilibrium degassing (Peterson et al., 2017; Dixon et al., 1995; Ghorso & Gualda, 2015). The H_2O/Cl and K/Cl ratios suggest that the DWF lavas assimilated with a similar brine-seawater mixture to the Fernandina and Sierra Negra group lavas from Peterson et al. (2017; ~10 wt% brine; Figure S4).

The spatial distributions of DWF lava compositions inferred from in situ sampling (from this study) are relatively consistent with the sparse sampling of the DWFs from previous dredging and rock cores (Geist et al., 2006). Rock core sample RC-04, collected from the deeper portion of DWF#1, is alkalic, while RC-05, collected midway up DWF#1, is tholeiitic in composition and similar to the DWF#1 tholeiites (Figure 3). Glass chips from dredge D-17 are bimodal and may have sampled both the underlying IF tholeiitic lavas and part of alkalic DWF#1 flow. Interestingly, RC-02, collected from DWF#2 is tholeiitic (Geist et al., 2006), while the ROV samples from this flow are alkalic (Figure 2). There is also a slight change in reflectivity in the side scan sonar (Figure 2) south of RC-02 that may indicate a flow boundary; however, without further sampling and observations this cannot be confirmed. Combined, these observations may indicate that DWF#2 is also composed of multiple flow units or that the rock core actually missed this flow and sampled the adjacent tholeiitic lavas (navigational precision of the rock core samples from Geist et al., 2006, was ~250 m).

These results suggest that what was previously mapped as a single lava flow in Geist et al. (2006) is likely composed of multiple eruptive events, which are required to produce distinct tholeiitic and alkalic compositions. No samples were collected from the middle of either flow, and there is no obvious transition between the two in the side scan sonar data. Therefore, due to a lack of sampling and visual observations, we cannot determine where the lavas transition from tholeiitic to alkalic. Further, without detailed observations of flow thickness and given uncertainty in preflow bathymetry, we do not attempt to calculate the total volume of either flow. However, large areal extent of the DWFs in MR-1 side scan data, and the presence of a ~30-m-deep collapse crater (Figure S2) within the shallow eastern region, is indicative of large volume eruptions, larger than previously inferred (Geist et al., 2006). Regardless, these studies show that magmas produced at the leading edge of the Galápagos plume are voluminous and compositionally heterogeneous, producing both tholeiitic and alkalic lava flows.

6.2. Origin of Tholeiitic Lavas

The DWF tholeiites collected in situ using the ROV and dredged on previous cruises are also compositionally similar to lavas erupted subaerially on Fernandina volcano (Figure 6), which is dominated by the eruption of relatively homogeneous tholeiitic basalts (Allan & Simkin, 2000; Geist et al., 2006; McBirney & Williams, 1969; White et al., 1993). Thermodynamic models indicate that subaerial Fernandina lava compositions are controlled by crystallization at relatively shallow depths (~2 km; Allan & Simkin, 2000). This is consistent with deformation studies (Geist et al., 2006) that suggest the presence of a shallow crustal magma chamber at these depths. Thus, the homogeneity of subaerially erupted basalts at Fernandina is attributed to efficient mixing and homogenization of melts in a shallow magma chamber prior to eruption (Allan & Simkin, 2000; Geist et al., 2014).

Based on compositional similarities, Geist et al. (2006) suggest that the submarine normal series tholeiitic lavas pass through Fernandina's magmatic plumbing system; however, greater phenocryst abundances in submarine Fernandina northwest rift zone lavas imply they may originate from greater depths within the Fernandina magma plumbing system (Geist et al., 2006; Geist et al., 2014). To determine if DWF tholeiites can be formed by crystallization of a mafic normal series basalt (Geist et al., 2006), fractional crystallization trends were modeled using MELTS version 1.0.1 (Ghiorso & Sack, 1995), via the alphaMELTS front end (Smith & Asimow, 2005). Calculations were run at 50 MPa, consistent with crystallization pressures estimated for the dredged normal series lavas (Geist et al., 2006) and the depth of the magma chamber inferred from deformation studies at Fernandina (~2 km; Allan & Simkin, 2000; Geist et al., 2006). A mafic basalt (NA064-074) was used as a parent composition for the models; water contents were varied (0.25, 0.5, and 1 wt%) with a starting oxygen fugacity of Quartz Fayalite Magnetite (QFM) + 0.5 (Peterson et al., 2015). Model runs were also carried out at QFM + 0.15 and 0.75, which spans the range predicted by Peterson et al. (2015), but there is no major effect on the modeling results (Figure S3). These models suggest that submarine DWF tholeiites can be formed by ~10% fractional crystallization of olivine, feldspar, and CPX from a mafic normal series basalt, while <5% crystallization of similar phases accounts for the variability observed within DWF basalts (Figure 3). Petrologic modeling and lava compositions strongly suggest that the previously identified submarine normal series tholeiites (Geist et al., 2006) and the DWF tholeiites sampled during the ROV dives are formed from similar petrogenetic processes, perhaps within the same magmatic system.

Plagioclase phenocrysts are common in both the subaerial (Allan & Simkin, 2000) and submarine tholeiitic lavas, but the submarine lavas also contain large olivine phenocrysts (~5%). Previous studies show that anorthite contents of the plagioclase and forsterite values of the olivine phenocrysts in the normal series are not in equilibrium with the host lavas, suggesting that the large phenocrysts in the dredged lavas are antecrysts that were entrained into the magma during eruption (Geist et al., 2006). The tholeiitic DWFs show similar phenocryst abundance to the dredged lavas, and there is no evidence for significant plagioclase crystallization in the trace element contents (e.g., no Eu anomaly and a weak negative Sr anomaly; Figure 5). Thus, our results are consistent with the hypothesis that the phenocryst-rich submarine DWF tholeiites are sourced from the dense olivine-rich crystal mush lower in the Fernandina magma plumbing system and erupt on the submarine flanks of the volcano via lateral dike and extrusion of lavas along the submarine rift zones (Geist et al., 2006).

Interestingly, the major and trace element contents are more variable in the IF tholeiitic lavas compared to the DWF tholeiites, and they have lower phenocryst abundances. Further, the IF lavas have variable

radiogenic isotope ratios (Figure 6), and based on sediment cover and lower reflectivity in side scan sonar data, the IF lavas are presumed older than the DWFs. This suggests that the mantle source feeding the lavas that erupted on the seafloor west of Fernandina has varied through time.

6.3. Origin of Alkalic Lavas

Alkalic lavas have been identified as a primary rock type erupted at the leading edge of the Hawaiian plume and are thought to form from lower extents of melting associated with the movement of the Pacific plate over the Hawaiian hotspot (Clague & Dalrymple, 1987; Coombs et al., 2006; Frey & Clague, 1983; Garcia et al., 1995; Moore et al., 1982). Similarly, alkalic basalts erupted at the youngest submarine Galápagos volcano (Roca Redonda; Figure 1) are thought to represent analogous juvenile stage volcanism on the northwest margin of the Galápagos plume (Standish et al., 1998). These alkalic lavas, which have high $[La/Sm]_N$ and $[Sm/Yb]_N$, are attributed to lower extents of mantle melting compared to tholeiitic lavas that are produced over the center of mantle upwelling (Standish et al., 1998). However, this is not the only mechanism that can produce alkalic magmas at ocean islands, including the Galápagos.

In addition to Roca Redonda, alkalic lavas have erupted on most of the Galápagos subaerial volcanoes (Naumann et al., 2002; White et al., 1993) and are represented in the high-K series lavas dredged from the seafloor west of Fernandina (Geist et al., 2006). Despite numerous studies, there is no consensus on how alkalic basalts are formed in the Galápagos; hypotheses include the following: (1) mantle source heterogeneity (Geist et al., 1986; Gibson et al., 2012; Harpp et al., 2014; Naumann et al., 2002; Standish et al., 1998), (2) high-pressure CPX crystallization (Geist et al., 1998; Naumann & Geist, 1999), (3) mixing of evolved and mafic magmas (Geist et al., 2006), and (4) variations in the extent of melting of a homogeneous mantle source (Geist et al., 1986; Naumann et al., 2002; Standish et al., 1998). These studies suggest that the complex tectonic setting of the Galápagos Islands and the Galápagos Spreading Center (GSC) to the north allow for a variety of processes to be involved in the formation of alkalic lavas in the Galápagos. In the following sections we evaluate each of these four mechanisms to determine the petrogenesis of alkalic DWF lavas.

6.3.1. Mantle Source

The Galápagos mantle plume is compositionally heterogeneous, and there are complex geochemical interactions with the upwelling depleted mantle beneath and nearby the GSC (Harpp & White, 2001; White et al., 1993). Four mantle sources have been identified in the Galápagos based on Sr, Nd, Pb, and He isotope ratios and $[La/Sm]_N$ ratios: (1) primitive lower mantle (PLUME), (2) depleted upper mantle (DUM), (3) enriched Floreana mantle (FLO), and (4) Wolf-Darwin lineament mantle (WD; Harpp & White, 2001; Hoernle et al., 2000). Mixing and melting of these end-member mantle components can account for a wide range of lava compositions (D. J. Geist et al., 1986; Gibson et al., 2012; Harpp et al., 2014; Harpp & White, 2001; Hemond et al., 1993; White et al., 1993), including alkalic basalts. For example, radiogenic isotope ratios suggest that eruption of both alkalic and tholeiitic magmas at Isla Santiago (Gibson et al., 2012) and San Cristobal (Geist et al., 1986; Figure 1) is at least partially attributed to melting of a heterogeneous mantle source. In both cases, alkalic lavas are produced by melting of a mantle source that contains a higher proportion of an enriched mantle component (PLUME) compared to depleted mantle (DUM), resulting in elevated trace element contents and more enriched radiogenic isotope ratios compared to the tholeiitic lavas, which are dominated by the DUM source (Geist et al., 1986; Gibson et al., 2012). Similarly, variations in mantle source has been suggested as an explanation for high $[La/Sm]_N$ and radiogenic isotope ratios reported at Floreana (Bow & Geist, 1992; Harpp et al., 2014).

These studies show that variations in mantle source may contribute to the formation of both alkalic and tholeiitic lavas over short spatial distances; however, unlike Isla Santiago or San Cristobal, the DWF basalts span very little of the compositional range observed in the Galápagos (Figure 6), with the exception of one IF tholeiitic sample (NA064-075). This suggests that both alkalic and tholeiitic DWFs are sourced from similar proportions of mixed mantle components. Based on $^{87}Sr/^{86}Sr$, $^{143}Nd/^{144}Nd$, $^{206}Pb/^{204}Pb$, $^{207}Pb/^{204}Pb$, $^{208}Pb/^{204}Pb$, and $[La/Sm]_N$, the mantle source for the alkalic and tholeiitic DWFs is primarily PLUME and DGM, nearly identical to the source of Fernandina's subaerial lavas (Figure 6). There may also be a small contribution by the FLO or WD component present in a higher proportion in Floreana and Northern Isabela subaerial lavas, respectively (Figure 6). These observations are consistent with isotopic studies of subaerial Fernandina lavas (Gibson & Geist, 2010; Harpp & White, 2001).

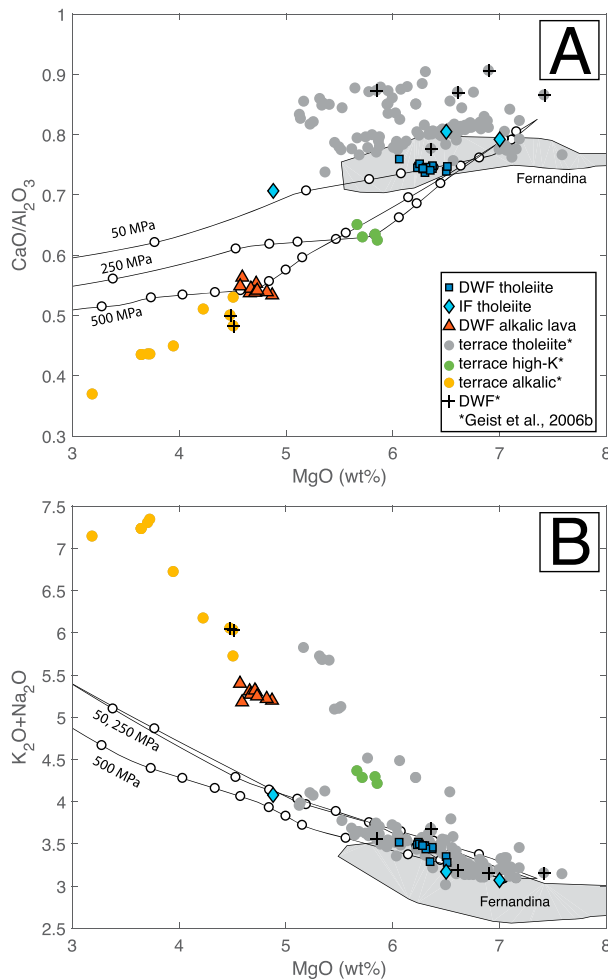


Figure 7. Magma evolution diagrams showing the effect of changing pressure on (a) CaO/Al₂O₃ and (b) total alkalis against MgO. Modeled fractional crystallization lines (black lines with white circles) generated from MELTs at 10, 50, and 250 MPa. White circles indicate 5% crystallization increments on each trend. See text for modeling details. DWF = deep-water lava flow; IF = interflow.

contents (particularly K₂O) and ratios are inconsistent with high-pressure CPX crystallization as a mechanism for the alkali enrichment of the DWFs (Figure 8b).

6.3.3. Magma Mixing

A third mechanism to produce alkalic lavas is by mixing an incompatible element enriched, highly evolved magma (rhyolite) with a depleted mafic magma (Geist et al., 2006). During crystallization, incompatible elements become enriched in the liquid phase. Thus, mixing of a highly evolved magma with a mafic magma can produce a range of intermediate compositions that are enriched in incompatible minor (K₂O) and trace element contents compared to the mafic lavas. Such mixing has been suggested by Geist et al. (2006) to explain the formation of the Galápagos submarine high-K series lavas dredged during the DRIFT4 cruise.

To determine if mixing can produce the DWF alkalic lavas, we calculate binary mixing trends (Figure 8) using the modeled fractional crystallization data from section 6.2 (H₂O = 0.5 wt%). A best fit mixture was chosen between two points along the modeled fractional crystallization trend, which best reproduced the K/Ti and MgO trend of the alkalic DWF and terrace lavas. The K/Ti ratios of the DWF alkalic lavas can be formed by mixing these mafic and evolved components in proportions of 80:20, respectively (Figure 8a). These proportions differ from estimates calculated by Geist et al. (2006; 48:52 mafic to evolved magma), which is consistent with the fact that the DWF alkalic lavas are more evolved (lower MgO contents) than the

Trace element ratios can also be affected by mantle source heterogeneity and variations in melting. At both San Cristobal and Santiago, incompatible trace elements correlate with the isotopic ratios, indicating that the degree of enrichment is controlled by source composition and variations in extent of melting (Geist et al., 1986; Gibson et al., 2012). However, the DWFs show no correlation between trace elements and radiogenic isotopes (Figure 6). A theoretical relationship between a global depleted mantle component (Workman & Hart, 2005) and primitive mantle component (Sun & McDonough, 1989) demonstrates the dependence of [La/Sm]_N and ¹⁴³Nd/¹⁴⁴Nd on mantle melting and mantle components (Figure S4). The lack of correlation between radiogenic isotope and trace element ratios (e.g., [La/Sm]_N and ¹⁴³Nd/¹⁴⁴Nd; Figure 6) indicates that mantle source heterogeneity does not contribute to the degree of enrichment in the DWF lavas (Geist et al., 1986; Gibson et al., 2012). Therefore, melts feeding eruptions of both alkalic and tholeiitic lava on the seafloor west of Fernandina are not controlled by variations in mantle source.

6.3.2. High-Pressure Fractional Crystallization

The formation of alkalic magmas can also be explained by high-pressure crystallization of CPX (Geist et al., 1998; Naumann & Geist, 1999; Wanless et al., 2006; Yoder & Tilley, 1962). At high pressures, the CPX liquidus expands at the expense of plagioclase and olivine, allowing for crystallization of CPX over a wider compositional range (Geist et al., 1998; Yoder & Tilley, 1962). High-pressure CPX fractionation depletes magmas of CaO, Sc, and SiO₂ while enriching the magma in alkalis, resulting in a decrease in CaO/Al₂O₃ ratios and the formation of alkalic compositions.

The submarine DWF alkalic lavas have lower CaO/Al₂O₃ (Figure 7a) compared to DWF tholeiitic lavas. This may indicate that the alkalic lavas are formed from high-pressure crystallization of CPX or variations in extents of melting. To determine if high-pressure crystallization can produce the alkalic compositions, we model fractional crystallization using the methods and parameters described in section 6.2 (H₂O = 0.5 wt%), varying pressure between 10 and 500 MPa, consistent with those estimated for the western Galápagos (Geist et al., 2006; Naumann & Geist, 1999). While high-pressure CPX crystallization can explain several of the major element trends (Figure 3), and CaO/Al₂O₃ (Figure 7a), it cannot explain the variation in total alkali contents (Figure 3a) or K/Ti between the alkalic and tholeiitic DWF samples (Figure 7b). The elevated incompatible minor element contents

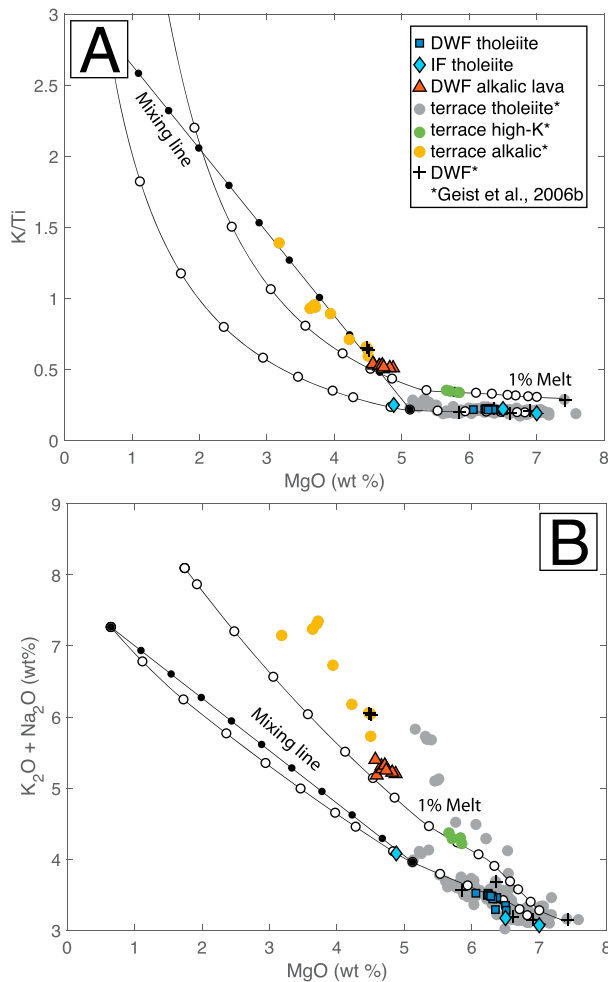


Figure 8. Effect of mixing and variations in extent of partial melting and fractional crystallization on (a) K/Ti versus MgO and (b) $[Sm/Yb]_N$. Modeled fractional crystallization lines in top figure (black lines with white circles) generated from MELTS starting from mafic tholeiite (NA064-074) and 1% (a and b) melt of Fernandina-like mantle (see text for model details). White circles indicate 5% crystallization increments on each trend. Black circles in top and bottom figures show the same hypothetical mixing trend between an evolved and mafic magma composition that reproduces the range in K/Ti versus MgO of alkalic DWF samples. See text for modeling details. Trace elements are modeled using alphaMELTS and the embedded partition coefficients (Smith & Asimow, 2005). DWF = deep-water lava flow; IF = interflow.

dredged high-K lavas. However, these proportions are inconsistent for other major element concentrations and ratios (Figures 8b and S3) and trace element ratios for elements that have similar compatibilities (e.g., $[Sm/Yb]_N$; Figure 9a). Thus, we conclude that it is unlikely that the mixing of evolved and mafic magmas, melted to the same extent and from the same source, results in the formation of the alkalic DWF lavas.

6.3.4. Variable Extents of Melting

Varying the extent of mantle melting, without changing the mantle source, can produce both alkalic and tholeiitic basalts at ocean islands (Frey et al., 1990, 1991; Geist et al., 1986, 1998; Moore et al., 1982; Naumann et al., 2002). During melting, highly incompatible elements (e.g., La) are initially highly enriched in the melt phase compared to less incompatible elements (e.g., Sm), but as the extent of melting increases, the highly incompatible trace elements are diluted. Further, deep melting in the presence of garnet is predicted to produce relatively low heavy rare earth element contents (i.e., high $[Sm/Yb]_N$; e.g., Gibson and Geist, 2010), due to the compatibility of heavy rare earths in garnet's crystal structure. Similar to $[La/Sm]_N$, high $[Sm/Yb]_N$ ratios are diluted as melting continues beyond the garnet stability field, which overwhelms the early $[Sm/Yb]_N$ enriched melts. Therefore, variations in the extent of melting of the same mantle source can produce both alkalic magmas with steep rare earth element patterns and tholeiitic basalts with flatter trace element patterns.

On the island of Isabela (Figure 1), systematic differences in the extent of melting of the same mantle source partially accounts for the variability of lava compositions erupted at Cerro Azul, Alcedo, and Sierra Negra volcanoes (Geist et al., 1995; Reynolds et al., 1995; Naumann et al., 2002). The highest $[La/Sm]_N$, indicative of the lowest extent of melting (2–3%), are found in lavas erupted at Cerro Azul, while Alcedo lavas have the lowest $[La/Sm]_N$, indicating higher extents of melting (~5%), and Sierra Negra has erupted lavas with intermediate $[La/Sm]_N$ ratios from ~4% melting (Naumann et al., 2002). Variation in $[La/Sm]_N$ ratios and inferred extents of melting are attributed to ~10–20 °C differences in mantle potential temperatures and lithospheric thickness variations beneath volcanoes on Isabela (Baker & Stolper, 1994; Gibson & Geist, 2010; Naumann et al., 2002), with the temperature and extent of melting decreasing (e.g., Cerro Azul) with distance from the center of plume upwelling or at greater lithospheric thicknesses (Gibson & Geist, 2010; Naumann et al., 2002).

To determine if variations in mantle melting can produce the range of trace element contents observed in the DWFs, we model mantle melting using pHMELTS (Asimow et al., 2004; Smith & Asimow, 2005). We use a

starting mantle composition of 20% primitive mantle (Jackson & Jellinek, 2013) and 80% depleted mantle (Workman & Hart, 2005) with water contents of 450 and 140 ppm, respectively (Peterson et al., 2017). Mixing proportions are taken from studies of subaerial Fernandina lavas due to the similarity in isotopic compositions (Figure 6) and are based on the volatile budget of the Galápagos mantle plume (Peterson et al., 2017). Models assume isentropic, polybaric near-fractional melting (0.5% melt retained) starting from 4 GPa and are modeled at mantle potential temperatures of 1460, 1500 and 1560 °C. These temperatures should correspond with a temperature of 1400–1500 °C using the alphaMELTS algorithm (Ghiorso et al., 2002) and span the range of what is predicted for the Galápagos mantle plume based on upper mantle shear wave velocity anomaly inversion (Villagómez et al., 2007). Fractional crystallization trends for trace element ratios at various extents of melting were modeled using the methods and parameters described in section 6.2 but using starting mafic alkalic and tholeiitic major element compositions from Geist et al. (2006).

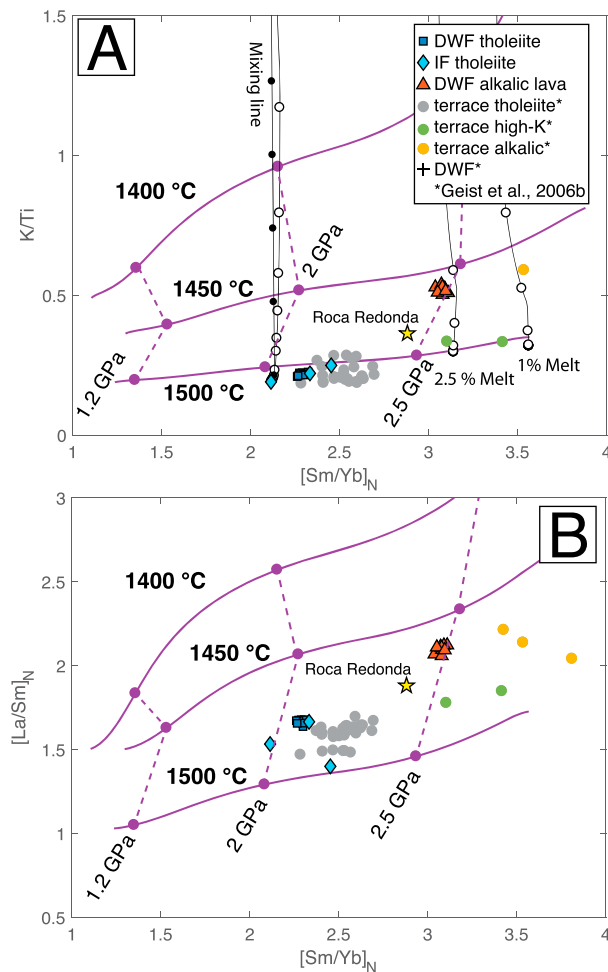


Figure 9. Effect of mixing and variations in extent of partial melting and fractional crystallization on (a) K/Ti versus $[Sm/Yb]_N$ and (b) $[La/Sm]_N$ versus $[Sm/Yb]_N$. Modeled fractional crystallization lines in top figure (black lines with white circles) generated from MELTS starting from mafic tholeiite (NA064-074) and 1%, 2.5%, and 5% melt of Fernandina-like mantle (see text for model details). White circles indicate 5% crystallization increments on each trend. Black circles in top and bottom figures show the same hypothetical mixing trend between an evolved and mafic magma composition that reproduces the range in K/Ti versus MgO of alkalic DWF samples. Purple lines indicate the evolution of the aggregated melt from the Fernandina-like mantle source at various pressures and melted at 1400, 1450, and 1500 °C. See text for modeling details. DWF = deep-water lava flow; IF = interflow.

Modeling results indicate that the variations between the major and trace element contents of the DWF alkalic and tholeiitic lavas can be explained by small variations (1–5%) in the extent of melting of the same mantle source (Figures 8 and 9). This is similar to other estimates for the formation of tholeiitic and alkalic magmas in the Galápagos (Naumann et al., 2002). In particular, the high total alkali contents, F/Nd ratios (Figure S4; Shimizu et al., 2016), and $[Sm/Yb]_N$, which is not modified by fractional crystallization (Figure 8b) can be explained by variations in the extent of melting of the same mantle source. To reproduce the observed trace element ratios in the alkalic DWF lavas compared to the tholeiitic ones, extents of melting must be modulated by a 500-MPa increase to the top of the melting column (for $[Sm/Yb]_N$) and decrease in mantle potential temperature by 25–50 °C.

A decrease in mantle potential temperature is expected for melts that are generated on the periphery of the mantle plume. A shorter melting column can be explained by a change in lithospheric thickness, incomplete mixing of melts from the entire melt column or mantle flow away from the plume center, which effectively truncates the melting column. We have made estimates for lithospheric thickness variations based on the average difference between $[Sm/Yb]_N$ between the DWF and alkalic lavas, which are 59 and 55 km, respectively (equation. 2; Gibson & Geist, 2010). Although this would explain the variation in degree of melting, it is unlikely that the lithospheric thickness varies by 4 km within such a short lateral distance and for lavas that have essentially erupted coevally. Thus, it is more likely that the alkalic lavas are produced from incomplete mixing or mantle flow at the edge of the plume.

6.4. Preferred Model for Origin of Deep-Water Flow Tholeiitic and Alkalic Lavas

There is no single model for the petrogenesis of alkalic lavas in the Galápagos. Alkalic lavas have been sampled on almost every major island (Naumann et al., 2002; White et al., 1993) and have been attributed to mantle source heterogeneity (Geist et al., 1986; Gibson et al., 2012; Harpp et al., 2014; Naumann et al., 2002; Standish et al., 1998), high-pressure CPX crystallization (Geist et al., 1998; Naumann & Geist, 1999), mixing of evolved and mafic magmas (Geist et al., 2006), and variations in the extent of melting of a homogeneous mantle source (Geist et al., 1986; Naumann et al., 2002; Standish et al., 1998). The range of processes involved in the formation of alkalic basalts is further complicated by the proximity of the upwelling plume to the GSC, resulting in spatial and temporal variability in the mantle source and lithospheric thickness.

Radiogenic isotope ratios indicate that the tholeiitic and alkalic basalts collected from the DWFs west of Fernandina are produced by melting of the same mantle source (similar to that of Fernandina; Figure 6); thus, source variability alone cannot account for the distinct lava compositions. Although there is evidence of high-pressure CPX crystallization (e.g., lower CaO/Al_2O_3 ratios; Figure 7), the elevated incompatible minor elements (e.g., K_2O and Na_2O) cannot be explained by crystallization from the same mantle source (Figure 7). Petrologic models show that mixing of a highly evolved rhyolitic magma and a mafic magma cannot produce the range of major or trace element contents observed in the DWF lavas (Figures 8b and 9a). Therefore, we suggest that the DWF alkalic basalts are formed from lower extents of melting of the Galápagos mantle source.

The submarine tholeiites are geochemically similar to the subaerial Fernandina tholeiites (e.g., Figure 6; Allan & Simkin, 2000; Geist et al., 2006), which are thought to form from higher extents of melting associated with

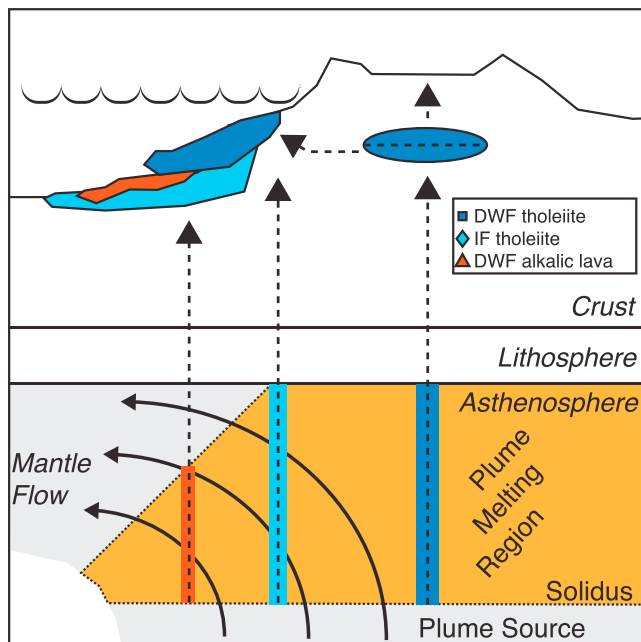


Figure 10. Schematic cartoon (not to scale) depicting the mantle processes responsible for generating the observed geochemical variations in the DWFs erupted at the base of the Galápagos platform west of Fernandina volcano. Radiogenic isotope ratios suggest that the alkalic and tholeiitic DWF lavas are produced by melting of the same mantle source. Tholeiitic lavas are produced by higher extents of melting beneath Fernandina. These highly phryc lavas are sourced from the cumulate-rich portion of the mush zone located lower in the magma chamber and erupt on the seafloor via lateral diiking through the submarine rift zone. By contrast, the phenocryst-poor alkalic lavas (and perhaps IF lavas) are produced by lower extents of melting at the leading edge of the mantle plume and bypass the magma chamber beneath Fernandina. DWF = deep-water lava flow; IF = interflow.

the center of the upwelling mantle plume (Figure 10). Abundant antecrysts suggest that the submarine tholeiites are sourced from or have passed through the dense crystal-rich mush zone at the bottom of the Fernandina magma chamber and that plagioclase and olivine crystals are entrained into the melt during lateral diiking beneath Fernandina's submarine rift zones (Geist et al., 2006; Geist et al., 2014). Thus, there is strong evidence that the DWF tholeiites are processed through the deeper portions of the Fernandina magmatic plumbing system. By contrast, the DWF alkalic lavas have subtly different Pb isotope ratios from those of Fernandina's subaerial lavas and the tholeiitic DWFs (Figure 6). The alkalic lavas are relatively aphyric compared to the submarine tholeiites, suggesting that they do not pass through the deeper crystal-rich portion of Fernandina's magmatic plumbing system during ascent to the seafloor. Instead, the alkalic magmas are formed from lower extents of melting at the leading edge of the Galápagos mantle plume, and these magmas appear to have bypassed the Fernandina magma chamber prior to their eruption on the seafloor west of the platform (Figure 10). IF tholeiites possess more chemical and isotopic variability and are less phenocryst rich than the DWF lavas, indicating that tholeiitic lavas may also periodically bypass Fernandina's shallow magmatic system and erupt onto the seafloor. The range of compositions and spatial distribution of DWF lavas suggests that tholeiitic and alkalic magmas can be produced and erupted within relatively short length scales at the leading edge of a mantle plume.

Alkalic basalts are also found at the leading edge of the Hawaiian plume, at Loihi Seamount, which is thought to represent the preshield stage of Hawaiian volcanism (Garcia et al., 1995). As the Pacific plate moves over the Hawaiian hotspot, the earliest eruptions are sourced from low-degree melts at the edge of the plume; however, as the plate continues to move over the hotspot, the extent of partial melting increases, resulting in eruption of tholeiitic lavas (Garcia et al., 1995). The alkalic basalts sampled from the DWFs west of Fernandina (by both our study and Geist et al., 2006) and lavas erupted at the youngest submarine volcano (Roca

Redonda; Standish et al., 1998) represent magmas formed by lower degrees of melting at the leading edge of the Galápagos plume as the Nazca plate moves over the center of upwelling. In this sense, the alkalic DWF magmas erupted on the seafloor west of the platform are similar to Loihi lavas derived from the preshield building stage of magmatism produced by low degrees of partial melting at the leading edge of a mantle plume. However, there is no large volcanic platform associated with the Hawaiian Islands.

Sampling suggests that the bulk of the ~3,000-m-thick Galápagos platform is likely composed of massive tholeiitic lava flows that coalesce to form the terraces (Geist et al., 2006, 2008). This is supported by side scan sonar data and ROV-based visual observations of relatively long (~10–20 km) DWFs and ~30-m-deep collapse craters (Figure S2). However, we suggest that at the leading edge of the plume, alkalic lavas may also contribute to the initial phases of platform construction. West of the center of plume upwelling, both alkalic and tholeiitic magmas can be produced contemporaneously and erupt on the relatively flat seafloor forming long lava flows. These compositionally variable lava flows eventually coalesce to form the terraces. The lack of alkalic lavas sampled from the platform walls likely reflects burial of the alkalic lavas by repeated eruption of tholeiitic lavas as the edge of the platform approaches the center of the mantle plume. Thus, both the alkalic and tholeiitic DWFs erupted at the leading edge of the plume are important components of the platform-building process in the Galápagos Archipelago.

Conclusion

Basaltic lavas from the DWFs on the seafloor west of Fernandina volcano are both alkalic and tholeiitic in composition. The alkalic lavas have elevated total alkali contents; high K/Ti, [Sm/Yb]_N, and [La/Sm]_N

ratios; and depleted MgO contents compared to the tholeiitic lavas. However, both the tholeiitic and alkalic lavas have similar radiogenic isotope ratios, indicating a similar mantle source. Petrologic modeling suggests that DWF alkalic magmas likely formed from various extents of partial melting of the same mantle source.

DWF tholeiitic lavas are likely part of the larger magmatic plumbing system that feeds subaerial eruptions in the western Galápagos on Fernandina and Isabela. Abundant phenocrysts suggest the tholeiites are sourced from or pass through the lower portion of the crystal-rich Fernandina magma chamber, as was suggested for other normal tholeiitic basalts dredged from the region (Geist et al., 2006). By contrast, the alkalic DWF lavas that are found at the western terminus of the lava flows are compositionally distinct and sparsely phyrlic, suggesting that they bypass the larger Fernandina magmatic system. Petrologic modeling suggests that the alkalic magmas are formed from lower extents of melting (1%) of the same mantle source compared to the tholeiitic magmas (5%). Eruption of alkalic lavas at the leading edge of the Galápagos mantle plume is consistent with models of volcanism at other ocean islands, where alkalic magmas are formed from lower extents of melting at the outer edges of the upwelling plume.

Our results add to the current model for Galápagos platform construction, which suggests that large flows coalesce into thick terraces that stack to form the Galápagos platform (Geist et al., 2006, 2008). Our data indicate that the large DWFs on the western edge of the platform are composed of multiple eruptive units, with variable compositions. We suggest that the alkalic lava flows form from lower extents of melting at the leading edge of the plume. While individual alkalic flows are relatively voluminous, they are not a primary lava type within the platform and are buried by much higher volume fluxes of tholeiitic volcanism as the Nazca plate migrates over the center of plume upwelling.

Acknowledgments

We thank the officers and crew of E/V *Nautilus* and ROV *Hercules*, the Ocean Exploration Trust shore-based and shipboard personnel, and Steve Carey (URI) for his assistance in documenting the lava samples at sea. We also thank Dr. Marion Lytle (BSU), Dr. Nick Bulloss (BSU), and Dr. George Kamenov (UF) for their assistance and training in geochemical analyses. This research was supported by the National Science Foundation (NSF) grant OCE-1634952 to V. D. Wanless, and the Boise State University Honors College. D. J. Fornari and S. A. Soule were supported in part by the Dalio Explore Fund at WHOI and WHOI's Independent Research & Development Fund. Additionally, we are grateful to the Galápagos National Park directorate and INOCAR for allowing the collection of submarine rock samples in collaboration with the Charles Darwin Research Foundation. Once published, data will be made available through EarthChem (<https://www.earthchem.org>).

References

- Allan, J. F., & Simkin, T. (2000). Fernandina volcano's evolved, well-mixed basalts: Mineralogical and petrological constraints on the nature of the Galápagos plume. *Journal of Geophysical Research*, *105*(B3), 6017–6041. <https://doi.org/10.1029/1999JB900417>
- Asimow, P. D., Dixon, J. E., & Langmuir, C. H. (2004). A hydrous melting and fractionation model for mid-ocean ridge basalts: Application to the Mid-Atlantic Ridge near the Azores. *Geochemistry, Geophysics, Geosystems*, *5*, Q01E16. <https://doi.org/10.1029/2003GC000568>
- Baker, M. B., & Stolper, E. M. (1994). Determining the composition of high-pressure mantle melts using diamond aggregates. *Geochimica et Cosmochimica Acta*, *58*(13), 2811–2827. [https://doi.org/10.1016/0016-7037\(94\)90116-3](https://doi.org/10.1016/0016-7037(94)90116-3)
- Bow, C. S., & Geist, D. J. (1992). Geology and petrology of Floreana Island, Galapagos Archipelago, Ecuador. *Journal of Volcanology and Geothermal Research*, *52*(1-3), 83–105. [https://doi.org/10.1016/0377-0273\(92\)90134-Y](https://doi.org/10.1016/0377-0273(92)90134-Y)
- Carey, B. S., Fisher, C. R., de Leon, P. S., Roman, C., Raineault, N. A., Suarez, J., et al. (2016). Exploring the undersea world of the Galápagos Islands. *Oceanography*, *29*(November), 32–34.
- Clague, D. A., & Dalrymple, G. B. (1987). The Hawaiian-Emperor volcanic chain. Part I. Geologic Evolution. In *Volcanism in Hawaii* (1350th ed., pp. 5–54). U.S. Geological Survey.
- Coombs, M. L., Sisson, T. W., & Lipman, P. W. (2006). Growth history of Kilauea inferred from volatile concentrations in submarine-collected basalts. *Journal of Volcanology and Geothermal Research*, *151*(1-3), 19–49. <https://doi.org/10.1016/j.jvolgeores.2005.07.037>
- Dixon, J. E., Stolper, E. M., & Holloway, J. (1995). An experimental study of water and carbon dioxide solubilities in mid-ocean ridge basaltic liquids. Part I: Calibration and solubility models. *Journal of Petrology*, *36*(6), 1607–1631.
- Fortin, M. A., Riddle, J., Desjardins-Langlais, Y., & Baker, D. R. (2015). The effect of water on the sulfur concentration at sulfide saturation (SCSS) in natural melts. *Geochimica et Cosmochimica Acta*, *160*, 100–116. <https://doi.org/10.1016/j.gca.2015.03.022>
- Frey, F. A., & Clague, D. A. (1983). Geochemistry of diverse basalt types from Loihi Seamount, Hawaii: Petrogenetic implications. *Earth and Planetary Science Letters*, *66*, 337–355. [https://doi.org/10.1016/0012-821X\(83\)90150-4](https://doi.org/10.1016/0012-821X(83)90150-4)
- Frey, F. A., Garcia, M. O., Wise, W. S., Kennedy, A., Gurriet, P., & Albareda, F. (1991). The evolution of Mauna Kea Volcano, Hawaii: Petrogenesis of tholeiitic and alkalic basalts. *Journal of Geophysical Research*, *96*(B9), 14,347–14,375. <https://doi.org/10.1029/91JB00940>
- Frey, F. A., Wise, W. S., Garcia, M. O., West, H., Kwon, S.-T., & Kennedy, A. (1990). Evolution of Mauna Kea Volcano, Hawaii: Petrologic and geochemical constraints on postshield volcanism. *Journal of Geophysical Research*, *95*(B2), 1271–1300. <https://doi.org/10.1029/JB095iB02p01271>
- Garcia, M. O., Foss, D. J. P., West, H. B., & Mahoney, J. J. (1995). Geochemical and isotopic evolution of Loihi volcano, Hawaii. *Journal of Petrology*, *37*(3), 729–1674. <https://doi.org/10.1093/petrology/37.3.729>
- Geist, D., Bergantz, G., & Chadwick, W. W. (2014). Galápagos magma chambers. In *The Galapagos: A natural laboratory for the Earth sciences*, (Vol. 204, pp. 55–70). Washington, DC: Geophysical Monograph.
- Geist, D., Chadwick, W., & Johnson, D. (2006). Results from new GPS and gravity monitoring networks at Fernandina and Sierra Negra Volcanoes, Galápagos, 2000-2002. *Journal of Volcanology and Geothermal Research*, *150*(1-3), 79–97. <https://doi.org/10.1016/j.jvolgeores.2005.07.003>
- Geist, D., Diefenbach, B. A., Fornari, D. J., Kurz, M. D., Harpp, K., & Blusztajn, J. (2008). Construction of the Galápagos platform by large submarine volcanic terraces. *Geochemistry, Geophysics, Geosystems*, *9*, Q03015. <https://doi.org/10.1029/2007GC001795>
- Geist, D., Howard, K. A., & Larson, P. (1995). The generation of oceanic rhyolites by crystal fractionation: The Basalt-Rhyolite association at Volcan Alcedo, Galapagos Archipelago. *Journal of Petrology*, *36*(4), 965–982.
- Geist, D., Naumann, T., & Larson, P. (1998). Evolution of Galápagos magmas: Mantle and crustal fractionation without assimilation. *Journal of Petrology*, *39*(5), 953–971. <https://doi.org/10.1093/petrology/39.5.953>
- Geist, D. J., Fornari, D. J., Kurz, M. D., Harpp, K. S., Soule, S. A., Perfit, M. R., et al. (2006). Submarine Fernandina: Magmatism at the leading edge of the Galápagos hot spot. *Geochemistry, Geophysics, Geosystems*, *7*, Q12007. <https://doi.org/10.1029/2006GC001290>

- Ghiorso, M. S., & Gualda, G. A. R. (2015). An H₂O–CO₂ mixed fluid saturation model compatible with rhyolite-MELTS. *Contributions to Mineralogy and Petrology*, 169(6), 53. <https://doi.org/10.1007/s00410-015-1141-8>
- Geist, D. J., McBirney, A. R., & Duncan, R. A. (1986). Geology and petrogenesis of lavas from San Cristobal Island, Galápagos Archipelago. *Geological Society of America Bulletin*, 97(5), 555–566. [https://doi.org/10.1130/0016-7606\(1986\)97<555:GAPOLF>2.0.CO;2](https://doi.org/10.1130/0016-7606(1986)97<555:GAPOLF>2.0.CO;2)
- Ghiorso, M. S., Hirschmann, M. M., Reiners, P. W., & Kress, V. C. (2002). The pMELTS: A revision of MELTS for improved calculation of phase relations and major element partitioning related to partial melting of the mantle to 3 GPa. *Geochemistry, Geophysics, Geosystems*, 3(5), 1030. <https://doi.org/10.1029/2001GC000217>
- Ghiorso, M. S., & Sack, R. O. (1995). Chemical mass transfer in magmatic processes IV. A revised and internally consistent thermodynamic model for the interpolation and extrapolation of liquid–solid equilibria in magmatic systems at elevated temperatures and pressures. *Contributions to Mineralogy and Petrology*, 119(2–3), 197–212. <https://doi.org/10.1007/BF00307281>
- Gibson, S. A., & Geist, D. (2010). Geochemical and geophysical estimates of lithospheric thickness variation beneath Galápagos. *Earth and Planetary Science Letters*, 300(3–4), 275–286. <https://doi.org/10.1016/j.epsl.2010.10.002>
- Gibson, S. A., Geist, D. G., Day, J. A., & Dale, C. W. (2012). Short wavelength heterogeneity in the Galápagos plume: Evidence from compositionally diverse basalts on Isla Santiago. *Geochemistry, Geophysics, Geosystems*, 13, Q09007. <https://doi.org/10.1029/2012GC004244>
- Glass, J. B., Fornari, D. J., Hall, H. F., Cougan, A. A., Berkenbosch, H. A., Holmes, M. L., et al. (2007). Submarine volcanic morphology of the western Galápagos based on EM300 bathymetry and MR1 side-scan sonar. *Geochemistry, Geophysics, Geosystems*, 8, Q03010. <https://doi.org/10.1029/2006GC001464>
- Goss, A. R., Perfit, M. R., Ridley, W. I., Rubin, K. H., Kamenov, G. D., Soule, S. A., et al. (2010). Geochemistry of lavas from the 2005–2006 eruption at the East Pacific Rise, 9°46'N–9°56'N: Implications for ridge crest plumbing and decadal changes in magma chamber compositions. *Geochemistry, Geophysics, Geosystems*, 11, Q05T09. <https://doi.org/10.1029/2009GC002977>
- Gregg, T. K. P., & Fink, J. H. (1995). Quantification of submarine lava morphologies through analog experiments. *Geology*, 23(1), 73–76. [https://doi.org/10.1130/0091-7613\(1995\)023<0073](https://doi.org/10.1130/0091-7613(1995)023<0073)
- Harpp, K. S., Geist, D. J., Koleszar, A. M., Christensen, B., Lyons, J., Sabga, M., et al. (2014). The geology and geochemistry of Isla Floreana, Galápagos: A different type of late-stage ocean island volcanism. *The Galapagos: A Natural Laboratory for the Earth Sciences*, 71–117. <https://doi.org/10.1002/9781118852538.ch6>
- Harpp, K. S., & White, W. M. (2001). Tracing a mantle plume: Isotopic and trace element variations of Galápagos seamounts. *Geochemistry, Geophysics, Geosystems*, 2(6). <https://doi.org/10.1029/2000GC000137>
- Hauri, E., Wang, J., Dixon, J. E., King, P. L., Mandeville, C., & Newman, S. (2002). SIMS analysis of volatiles in silicate glasses 1. Calibration, matrix effects and comparisons with FTIR. *Chemical Geology*, 183(1–4), 99–114. [https://doi.org/10.1016/S0009-2541\(01\)00375-8](https://doi.org/10.1016/S0009-2541(01)00375-8)
- Hemond, C., Arndt, N. T., Lichtenstein, U., Hofmann, A. W., Oskarsson, N., & Steinthorsson, S. (1993). The heterogeneous Iceland plume: Nd–Sr–O isotopes and trace element constraints. *Journal of Geophysical Research*, 98(B9), 15833. <https://doi.org/10.1029/93JB01093>
- Hoernle, K., Werner, R., Morgan, J. P., Garbe-schonberg, D., Bryce, J., & Mrazek, J. (2000). Existence of complex spatial zonation in the Galapagos plume for at least 14 m.y. *Geology*, 28(5), 435–438. [https://doi.org/10.1130/0091-7613\(2000\)28<435:Eoczi>2.0.Co;2](https://doi.org/10.1130/0091-7613(2000)28<435:Eoczi>2.0.Co;2)
- Jackson, M. G., & Jellinek, A. M. (2013). Major and trace element composition of the high ³He/⁴He mantle: Implications for the composition of a nonchondritic Earth. *Geochemistry, Geophysics, Geosystems*, 14, 2954–2976. <https://doi.org/10.1002/ggge.20188>
- Kelley, K. A., Plank, T., Ludden, J., & Staudigel, H. (2003). Composition of altered oceanic crust at ODP sites 801 and 1149. *Geochemistry, Geophysics, Geosystems*, 4(6), 8910. <https://doi.org/10.1029/2002GC000435>
- Lipman, P. W., & Calvert, A. T. (2013). Modeling volcano growth on the island of Hawaii: Deep-water perspectives. *Geosphere*, 9(5), 1348–1383. <https://doi.org/10.1130/GES00935.1>
- Lytle, M. L., Kelley, K. A., Hauri, E. H., Gill, J. B., Papia, D., & Arculus, R. J. (2012). Tracing mantle sources and Samoan influence in the north-western Lau back-arc basin. *Geochemistry, Geophysics, Geosystems*, 13, Q10019. <https://doi.org/10.1029/2012GC004233>
- MacDonald, G. A., & Katsura, I. (1964). Chemical composition of Hawaiian Lavas. *Journal of Petrology*, 5, 82–133. <https://doi.org/10.1093/petrology/5.1.82>
- McBirney, A. R., & Williams, H. (1969). *Geology and petrology of the Galápagos Islands*. Boulder, CO: Geological Society of America.
- McDonough, W. F., & Sun, S.-S. (1995). Composition of the Earth. *Chemical Geology*, 120, 223–253. [https://doi.org/10.1016/0009-2541\(94\)00140-4](https://doi.org/10.1016/0009-2541(94)00140-4)
- Moore, J. G., Clague, D. A., & Normark, W. R. (1982). Diverse basalt types from Loihi seamount, Hawaii. *Geology*, 10(2), 88–92. [https://doi.org/10.1130/0091-7613\(1982\)10<88:DBTFLS>2.0.CO;2](https://doi.org/10.1130/0091-7613(1982)10<88:DBTFLS>2.0.CO;2)
- Naumann, T., Geist, D., & Kurz, M. (2002). Petrology and geochemistry of Volcán Cerro Azul: Petrologic diversity among the Western Galápagos volcanoes. *Journal of Petrology*, 43(5), 859–883. <https://doi.org/10.1093/petrology/43.5.859>
- Naumann, T. R., & Geist, D. J. (1999). Generation of alkalic basalt by crystal fractionation of tholeiitic magma. *Geology*, 27(5), 423–426. [https://doi.org/10.1130/0091-7613\(1999\)027<0423:GOABBC>2.3.CO;2](https://doi.org/10.1130/0091-7613(1999)027<0423:GOABBC>2.3.CO;2)
- Perfit, M., Wanless, V. D., Ridley, W. I., Klein, E., Smith, M., Goss, A., et al. (2012). Lava geochemistry as a probe into crustal formation at the East Pacific Rise. *Oceanography*, 25(1), 89–93. <https://doi.org/10.5670/oceanog.2012.06>
- Peterson, M. E., Kelley, K. A., Cottrell, E., Saal, A. E., & Kurz, M. D. (2015, December). The oxidation state of Fe in glasses from the Galapagos Archipelago: Variable oxygen fugacity as a function of mantle source. In *AGU Fall Meeting Abstracts*.
- Peterson, M. E., Saal, A. E., Kurz, M. D., Hauri, E. H., Blusztajn, J. S., Harpp, K. S., et al. (2017). Submarine basaltic glasses from the Galapagos Archipelago: Determining the volatile budget of the mantle plume. *Journal of Petrology*, 58(7), 1419–1450. <https://doi.org/10.1093/petrology/egx059>
- Reynolds, R. W., & Geist, D. J. (1995). Petrology of lavas from Sierra Negra volcano, Isabela Island, Galápagos archipelago. *Journal of Geophysical Research*, 100(B12), 24,537–24,553. <https://doi.org/10.1029/95JB02809>
- Rognstad, M. (1992). Hawaii MR1: A new underwater mapping tool. International Conference on Signal Processing and Technology (pp. 900–905). DSP Associates, Newton, MA. Retrieved from <http://www.soest.hawaii.edu/HMRG/facstaff/mark/MR1Paper.pdf>
- Saal, A. E., Kurz, M. D., Hart, S. R., Blusztajn, J. S., Blichert-Toft, J., Liang, Y., et al. (2007). The role of lithospheric gabbros on the composition of Galapagos lavas. *Earth and Planetary Science Letters*, 257(3–4), 391–406. <https://doi.org/10.1016/j.epsl.2007.02.040>
- Schwartz, D. M., Wanless, V. D., Berg, R., Jones, M., Fornari, D. J., Soule, S. A., et al. (2018). Petrogenesis of alkalic seamounts on the Galápagos Platform. *Deep-Sea Research Part II: Topical Studies in Oceanography*, 150, 170–180. <https://doi.org/10.1016/j.dsr2.2017.09.019>
- Shimizu, K., Saal, A. E., Myers, C. E., Nagle, A. N., Hauri, E. H., Forsyth, D. W., et al. (2016). Two-component mantle melting-mixing model for the generation of mid-ocean ridge basalts: Implications for the volatile content of the Pacific upper mantle. *Geochimica et Cosmochimica Acta*, 176, 44–80. <https://doi.org/10.1016/j.gca.2015.10.033>
- Smith, P. M., & Asimow, P. D. (2005). Adiabatic-1ph: A new public front-end to the MELTS, pMELTS, and pHMELTS models. *Geochemistry, Geophysics, Geosystems*, 6, Q02004. <https://doi.org/10.1029/2004GC000816>

- Standish, J., Geist, D. J., Harpp, K., & Kurz, M. D. (1998). The emergence of a Galápagos shield volcano, Roca Redonda. *Contributions to Mineralogy and Petrology*, 133(1–2), 136–148. <https://doi.org/10.1007/s004100050443>
- Sun, S. -s., & McDonough, W. F. (1989). Chemical and isotopic systematics of oceanic basalts: Implications for mantle composition and processes. *Geological Society, London, Special Publications*, 42(1), 313–345. <https://doi.org/10.1144/GSL.SP.1989.042.01.19>
- Villagómez, D. R., Toomey, D. R., Hooft, E. E. E., & Solomon, S. C. (2007). Upper mantle structure beneath the Galápagos Archipelago from surface wave tomography. *Journal of Geophysical Research*, 112, B07303. <https://doi.org/10.1029/2006JB004672>
- Wanless, V. D., Garcia, M. O., Rhodes, J. M., Weis, D., & Norman, M. D. (2006). Shield-stage alkalic volcanism on Mauna Loa Volcano, Hawaii. *Journal of Volcanology and Geothermal Research*, 151(1–3), 141–155. <https://doi.org/10.1016/j.jvolgeores.2005.07.027>
- White, W. M., McBirney, A. R., & Duncan, R. A. (1993). Petrology and geochemistry of the Galápagos Islands: Portrait of a pathological mantle plume. *Journal of Geophysical Research*, 98(B11), 19,533–19,563. <https://doi.org/10.1029/93JB02018>
- Workman, R. K., & Hart, S. R. (2005). Major and trace element composition of the depleted MORB mantle (DMM). *Earth and Planetary Science Letters*, 231(1–2), 53–72. <https://doi.org/10.1016/j.epsl.2004.12.005>
- Yoder, H. S., & Tilley, C. E. (1962). Origin of basalt magmas: An experimental study of natural and synthetic rock systems. *Journal of Petrology*, 3(3), 342–532. <https://doi.org/10.1093/petrology/3.3.342>